Adaptation of centromere to breakage through local genomic and epigenomic remodeling in wheat

Jingwei Zhou, Yuhong Huang, Huan Ma, et al.

Genome Res. published online September 30, 2025
Access the most recent version at doi:10.1101/gr.280913.125

Adaptation of centromere to breakage through local genomic and epigenomic remodeling in wheat

Author affiliations:

Jingwei Zhou[1#], Yuhong Huang[1,2#], Huan Ma[1], Yiqian Chen[1], Chuanye Chen[1], Fangpu Han[3,4], Handong Su[1,2*]

[1] National Key Laboratory of Crop Genetic Improvement, Hubei Hongshan Laboratory, Huazhong Agricultural University, Wuhan, 430070, China

[2] Shenzhen Branch, Guangdong Laboratory for Lingnan Modern Agriculture, Genome Analysis Laboratory of the Ministry of Agriculture, Agricultural Genomics Institute at Shenzhen, Chinese Academy of Agricultural Sciences, Shenzhen, 518120, China

[3] State Key Laboratory of Plant Cell and Chromosome Engineering, Institute of Genetics and Developmental Biology, Innovation Academy for Seed Design, Chinese Academy of Sciences, Beijing, 100101, China

[4] University of the Chinese Academy of Sciences, Beijing 100049, China

[#] These authors contribute equally to this work

[*] Corresponding authors: Handong Su

Dr. Handong Su (Email: shandong@mail.hzau.edu.cn)

National Key Laboratory of Crop Genetic Improvement, Hubei Hongshan Laboratory, Huazhong Agricultural University, Wuhan, 430070, Hubei, China

Running title: How damaged centromeres preserve functional integrity

Abstract

Centromeres, characterized by their unique chromatin attributes, are indispensable for safeguarding genomic stability. Due to their intricate and fragile nature, centromeres are susceptible to chromosomal rearrangements. However, the mechanisms preserving their functional integrity and supporting nucleus homeostasis following breakages remained enigmatic. In this study, we use wheat ditelosomic stocks, which arise from centromere breakage, to explore the genetic and epigenetic alterations in damaged centromeres. Our investigations suggest novel chromosome end structures marked by *de novo* addition of telomeres, as well as localized chromosomal shattering, including segment deletions and duplications near centromere breakpoints. We reveal that the damaged centromeres possess a remarkable capacity for self-regulation, through employing structural modifications such as expansion, contraction, and neocentromere formation to maintain their functional integrity. Centromere breakage triggers nucleosome remodeling and is accompanied by local transcription changes and chromatin reorganization, and subsequently may contribute to the stabilization of broken chromosomes. Our findings highlight the resilience and adaptability of plant chromosomes in response to centromere breakage, and provide valuable insights into the stability of centromeres, thereby offering promising prospects to manipulate centromeres for targeted chromosomal innovation and crop genetic improvement.

Keywords: Wheat; Centromere breakage; Genomic and epigenomic reorganizations; CENH3; Stabilization

Introduction

Chromosomal stability is a crucial prerequisite for the accurate transmission of genetic information during cell division. Disruptions to chromosomes, whether spontaneous or induced by external agents, often result in abnormal cell division and aneuploidy, conditions frequently observed in cancer cells (Bakhoum and Cantley 2018). Moreover, chromosome rearrangements post-DNA breakage are well-documented and contribute significantly to genome evolution and the development of key agronomic traits in crops (Willson 2020). Comparative genomics studies have demonstrated that speciation often involves chromosome karyotype changes, such as chromosome end fusions or the insertion of one chromosome near another's centromere (Mandakova et al. 2020; Lysak 2022). Chromosomes exhibit homeostatic flexibility, naturally readjusting their structural and nuclear organization to resist breakage events (Pentzold et al. 2021; Zagelbaum et al. 2023). Therefore, understanding the effects of chromosome breakage is crucial for unraveling the intricacies of genome homeostasis in evolution and speciation.

Centromeres, as vital components of chromosomes, play a critical role in maintaining the overall stability of genome architecture (Hofstatter et al. 2022; Zhou et al. 2022). Recent advancements have revealed that centromeres are vulnerable to breakage due to their repetitive nature (Barra and Fachinetti 2018; Chen et al. 2024). This vulnerability is compounded by the frequent occurrence of DNA strand breaks within active human core centromeres, resolved by the evolutionarily conserved RAD51 recombinase (Saayman et al. 2023). Dysfunctions at centromeres can lead to diverse chromosomal rearrangements, ultimately driving karyotype evolution and speciation over time (Lu and He 2019; Yadav et al.

2020). A CRISPR-based method was developed to engineer human cells with distinct and innovative karyotypes, enabling to induce chromosome-specific aneuploidy (Bosco et al. 2023).

Centromeres harbor a high level of mechanical stress or tension as microtubules exert pulling forces on the centromere-kinetochore complexes, which is essential for accurate chromosome segregation (Barra and Fachinetti 2018; Bloom 2024; Kolbin et al. 2025). Univalent chromosomes tends to transverse misdivision splits near centromeric regions, forcing the chromosome into a tug-of-war in a process called centromere misdivision (Darlington 1939). This process can lead to the formation of telocentric chromosomes, isochromosomes, and potential Robertsonian translocations in plant (Lukaszewski 2010; Koo et al. 2015; Kopecky and Lukaszewski 2019). Telomeres, protecting linear chromosome ends, are essential for the normal transmission of chromosomes (Blackburn et al. 2015). Following post-centromere misdivision, it requires the attachment of new telomeres and the adaptation of the damaged centromere to form stable telocentric structures (Birchler and Han 2018). The details become murky after that, with few resolved instances of centromere breakage and subsequent repair events to maintain genomic structure and function.

Allohexaploid wheat exhibits remarkable tolerance to chromosome restructuring (Levy and Feldman 2022). Recent telomere-to-telomere genome assemblies have revealed that functional centromeres in wheat, average 10.2 Mb in size and are predominantly composed of specific Gypsy-type retrotransposons (Liu et al. 2025; Wang et al. 2025). Wheat telocentric lines were initially derived from centromere breakages in monosomic lines, resulting from chromosome misdivision or isochromosomes in Chinese Spring (CS) (Sears 1954). A

complete set of mono/di-telocentrics has been created for the 21 wheat chromosomes, serving as vital genetic stocks for gene allocation to specific chromosome arms (Kiesselbach 1949; Gill et al. 1999). These genetic materials are invaluable for examining the consequences of centromere dysfunction, playing a critical role in wheat genetics research. In this study, we investigate the molecular DNA-level processes underlying centromere breakage in wheat. Our goal is to provide insights into how centromeres maintain their structural and functional integrity to ensure chromosome stability, and to shed light on the complex structures of newly formed chromosome ends in nature.

Results

Reconstruction of chromosome end structure via *de novo* telomere addition following centromere misdivision in wheat

To investigate the consequences of centromere breakage on wheat genomic architecture, we analysis the CS ditelosomic (CSDt) lines from homoeologous group 1, 6, and 7 chromosomes. Cytogenetic analysis confirmed the presence of telosomic chromosomes carrying either the short or long arm (Supplemental Fig. S1). Telomeric signals were observed at the terminal breakpoints of the telosomic chromosomes (Fig. 1A), suggesting *de novo* addition of telomeres at chromosome ends following centromere misdivision (Putnam et al. 2004; Tan et al. 2024). However, other mechanisms, including chromosome fusion followed by breakage-fusion-bridge (BFB) cycles, or the capture of existing telomeric sequences, could also contribute to stabilize these broken ends (McClintock 1939; Zeng et al. 2025). Further karyotype analysis using pTa535-1 and pSc119.2 repeat probes with chromosome-specific

patterns (Tang et al. 2014) revealed no major chromosomal rearrangements but identified terminal deletions on Chr2B in Dt6BS and Chr3B in Dt6BL lines (Supplemental Fig. S2). The lack of subtelomeric repeat signals at the break ends provides suggestive evidence for chromosome end reconstructions following centromere breakage (Supplemental Fig. S2). Multicolor fluorescence *in situ* hybridization (Multi-FISH) further confirmed the absence of inter-chromosomal homoeologous exchanges (Supplemental Fig. S3). Observations of meiotic progression in pollen mother cells demonstrated that the telocentric chromosomes underwent meiosis with normal pairing or segregation patterns, comparable to intact chromosomes (Supplemental Fig. S4). These observation of cytological normal divisions and stable chromosome transmission suggests that broken chromosomal ends have been stabilized.

To further elucidate these events, we performed analysis of centromeric signal (CRW) intensities between telosomic chromosomes and their intact counterparts in CS. In general, telosomic chromosomes exhibited reduced signal intensities (Fig. 1A-B, Supplemental Fig. S1), consistent with previous reports that centromeric DNA loss during misdivision (Koo et al. 2015; Guo et al. 2016). Residual centromeric signals were predominantly localized at the breakpoints of long-arm telosomes (1AL, 1BL, 6AL, 6BL, and 7BL), with weaker signals on short-arm telosomes (1AS, 7BS, and 7DS). No obvious CRW signals were detected on 1BS, 1DS, 1DL, 6AS, 6BS, 6DS, 6DL, 7AS, 7AL, and 7DL telosomes (Fig. 1A-B). Previous findings revealed that stronger centromeric repeat signals are associated with enhanced kinetochore assembly and spindle microtubule interactions (Chmatal et al. 2014; Iwata-Otsubo et al. 2017). The stronger centromere-associated signals were retained in the

long arm of broken chromosomes (Fig. 1C), which might predispose breakpoints to occur more frequently toward short arms. Collectively, our findings suggest that centromere misdivision may involve one or multiple breakpoints flanking the original centromere on one or both sides.

Localized complex chromosome variations occurred near damaged centromere following misdivision

To map the landscape of centromere breakages in CSDt lines, we performed whole-genome resequencing at approximately 5× coverage. Sequencing reads were aligned to the near-complete CS reference genome assembly (Wang et al. 2025), and the coverage depths were assessed in 20-Mb chromosomal windows. Beyond previously reported terminal deletions in Dt1BS and Dt6BS (Devos et al. 1999), we identified a 10.98-Mb terminal duplication (Chr7A: 700,155,901–711,135,851) in Dt1BS, and a terminal deletion (Chr3D: 1–46,032,549) in Dt6BL (Supplemental Fig. S5A-C). Moreover, large interstitial duplications near CEN1B (37.7-Mb and 7.2-Mb) were detected in Dt7BS and Dt7BL lines, respectively (Supplemental Fig. S5C).

We divided the centromeric regions into consecutive 1-kb windows and identified breakpoint-associated regions by analyzing variations in resequencing coverage depth across these windows, detecting a total of 40 such regions across 18 ditelosomic lines (Supplemental Table S1). Overall, the chromosomes break primarily within core centromere (6 out of 9 chromosomes) or adjacent pericentromere (Fig. 2A-C, Supplemental Fig. S6A-C). Further examination of CENH3 binding within the breakpoint-associated regions revealed enrichment levels comparable to centromeric average (Supplemental Fig. S6D), suggesting that breakage

occur within active centromeric chromatin. These broken ends often exhibited localized deletions, terminal fragment amplifications, and discontinuous fragment fusions (Fig. 2A-C). For instance, in the Dt1BS line, the chromosome break occurred 17.8 Mb distal to the right of centromere, and was associated with complete loss of the original centromere and a 1.66-Mb terminal amplification (Chr1B: 243,980,011–245,644,800). In the Dt1BL line, several breakpoints, either simultaneous or sequential, led to the loss of most original centromere (Fig. 2A, middle). Segment presence or absence was validated using PCR with region-specific primers (Fig. 2D, Supplemental Fig. S7 and Supplemental Table S2). Furthermore, terminal fragment duplications were detected at the distal break ends of chromosomes in 9 out of 18 ditelosomic lines, with additional internal terminal amplifications observed (Fig. 2A-C). These copy number increases were quantified using resequencing data and validated by quantitative PCR (Fig. 2E-F). These subtelomeric duplications were aligned with the hallmark of BFB cycles or break-induced replication (BIR) model (Kim et al. 2021; Showman et al. 2024), suggestive of breakage-induced end restructuring.

To extend our findings, we analyzed 20 publicly available resequencing datasets from CS ditelosomic lines with approximately 100.5× sequencing coverage ((IWGSC) 2014), which corroborated the occurrence of complex structural variations, particularly in the B subgenome, which exhibited greater complexity than the A and D subgenomes. Similar patterns of centromere breakpoints and localized rearrangements were observed across multiple lines (Supplemental Fig. S8). These results indicate how centromere misdivision initiates cascading localized chromosomal fragmentation and reorganization. The consistent rearrangement patterns adjacent to breakpoints, suggest the maintenance of genomic stability following

centromere breakage across generations.

Remodeling of centromere architecture following breakage in wheat ditelosomic lines

To investigate how centromere structure and function respond to damage from chromosome breakages and following generations, we conducted CENH3 ChIP-seq experiments on CSDt lines and compared their binding profiles to CS wheat. Our ChIP-seq results revealed that in most cases, CENH3 enrichments remained at or near their original positions, while centromeres on other intact chromosomes showed no significant alterations (Supplemental Fig. S9). The residual centromeres retained their original CENH3-enriched domains in eight telocentric chromosomes (1AS, 1AL, 1DL, 6AS, 6DL, 7BS, 7DS and 7DL), which we defined as “maintained” centromeres (Fig. 3A, Supplemental Fig. S10). Conversely, in the Dt6BL line, a large segment of the original centromere was lost during misdivision process, resulting in a 1.1-Mb reduction from the left side of the centromere, shrinking its total size to 1.5-Mb (Chr6B: 347,247,275–348,786,174) (Fig. 3B). Despite this shrinkage, these small centromeres appeared sufficient for kinetochore assembly and telosomic chromosomes transmission, suggesting their remarkable structural resilience.

We identified six instances where residual CENH3-binding domains underwent expansion after breakage, covering regions between 975.5 kb to 3.46 Mb (Fig. 3C, Supplemental Fig. S10). For example, in Dt1BL, the centromere-adjacent breakpoint was associated with the loss of most original centromeric sequence simultaneously or subsequently (Chr1B: 238,133,951–243,329,818), followed by a 976.4-kb amplification toward the left arm (Fig. 3C). In the Dt1DS line, only 662.3-kb of the original centromere remained, which might be

insufficient to maintain proper kinetochore integrity for a ~170 Mb telosomic chromosome. The centromere expanded 294.4 kb leftward, now spanning 1.96 Mb (Chr1D: 171,459,145–173,415,900), partially incorporating adjacent pericentromeric region (Supplemental Fig. S10B). These results suggest that centromere expansion occurs more frequently than contraction after breakage, and such expansion may compensate for insufficient residual domains, allowing centromere to reach a size optimized for telocentric chromosome transmission.

To assess changes in CENH3 nucleosome distribution after centromere misdivision, we analyzed ChIP-seq fragment distributions, and found CENH3 nucleosome patterns in damaged centromeres differed from their shared counterpart domains in CS (Fig. 3A-C, Supplemental Fig. S10). Pearson correlation coefficients range from 0.44 to 0.83, which was significantly lower than the values observed for centromeres on other structurally normal chromosomes (Fig. 3D, upper corner, Supplemental Fig. S11A). Correlation values near localized structural variations did not differ substantially from those in stable regions (Fig. 3D, lower corner), suggesting that chromosome breakages, rather than local structural changes, may contribute more significantly to altered centromeric nucleosome landscapes. Dinucleotide composition surrounding CENH3 nucleosome centers in reorganized centromeres remained largely consistent with that of CS wheat (Fig. 3E, Supplemental Fig. S11B). Similarly, CENH3 nucleosome positioning on the CRW was largely preserved across most ditelosomic chromosomes, indicating that nucleosome phasing is independent of structure remodeling (Fig. 3F). Overall, these results point to a degree of structural plasticity to genomic stress in wheat centromeres, although the mechanisms remain to be fully

characterized.

De novo centromeres form in acentric chromosome fragments following complex structural rearrangements

We explored three scenarios where chromosome breakages resulted in telocentric chromosomes lacking their original centromeres, and in each case, we observed the emergence of a new CENH3-binding domain near pericentromeric regions (Fig. 4A). On Chr1BS, a neocentromere emerged approximately 650-kb distal to the original centromere, covering a roughly 1.88 Mb domain (243.98-245.86 Mb) (Fig. 4B, left). On Chr6BS, a small remnant near the original centromere (578-kb) was detected, but a larger 1.72 Mb CENH3 domain emerged 23.3 Mb away (321.07–322.79 Mb), possibly through the re-ligation of two subdomains (Fig. 4B, middle). Similarly, on Chr7AS, a neocentromere was observed 1.04 Mb upstream of the original centromere, covering a 4.58 Mb region between 361.93–366.51 Mb (Fig. 4B, right). These examples illustrate how centromere breakages and subsequent structural changes can induce neocentromere formation, which may be essential for rescuing acentric fragments.

DNA feature analysis indicates that neocentromeres exhibited lower gene content but higher transposable element (TE) density (Fig. 4C). Several genes were located near the boundaries of these neocentromeres (Dt1BS: G1, G6; Dt6BS: G14; Dt7AS: G15 and G23), suggesting that large gene architectures or transcriptional activity may restrict CENH3 expansion and centromere formation in adjacent regions (Fig. 4B). Transcription of genes (Dt7AS: G15 and G23) within these regions might hinder seeding and spreading of CENH3, prior to centromere

establishment (Fig. 4B-D). To explore the epigenetic context before neocentromere formations, we examined DNA methylation levels in CS, and these regions exhibited relatively lower DNA methylation levels (Fig. 4E). However, the presence of H3K9me2 in neocentromeric regions prior to centromere establishment supports that neocentromere formation preferentially occurs in heterochromatic, gene-sparse regions (Supplemental Fig. S12A). Moreover, CENH3 nucleosome positioning on CRW sequences varied widely in different neocentromeres (Supplemental Fig. S12B-C), suggesting structural organization even within these newly formed centromeres. These findings suggest that while neocentromeres retain essential functions, their chromatin organization may differ from canonical centromeres.

Concerted local open chromatin and transcriptional dynamics contribute to genomic stabilization following centromere misdivision

To investigate how gene expression and chromatin structure respond to centromere breakage, we conducted RNA-seq and ATAC-seq assays on these ditelosomic lines and CS wheat. In total, we identified 34 upregulated and 29 downregulated genes within the (peri)centromeric regions of ditelosomic lines relative to CS counterparts (Fig. 5A, Supplemental Fig. S13 and Supplemental Table S3). The majority of these genes (59 out of 63) were located in pericentromeric regions, with only four situated in core centromere (Supplemental Table S3). Analysis of chromatin accessibility indicated that the downregulated genes in ditelosomic lines coincided with reduced chromatin openness, while upregulated genes maintained a consistent level of accessibility (Fig. 5B and Supplemental Fig. S14A-B), suggesting some

complicated genes were influenced by both chromatin openness and CENH3 enrichment. For instance, in amplified centromere of Dt7BL, gene *TraesCS7B01G273700*, originally located at centromere boundary, became repositioned to a CENH3-depleted subdomain. Its expression significantly increased in Dt7BL compared to CS, accompanied by elevated promoter accessibility (Fig. 5C). In contrast, in stable centromere of Dt7DS, *TraesCS7D01G418600* expression declined markedly with no chromatin accessibility (Supplemental Fig. S14B). CENH3-binding levels at these loci remained largely unchanged, indicating that internal structural rearrangements may drive chromatin reorganization, which in turn modulate gene activity. We then compared open chromatin sates in (peri)centromeric regions before and after centromere damage. Expanded centromeric domains remodeled to adopt a more open configuration, while contracted domains become more compact in CSDt lines (Fig. 5D). These findings indicated that centromeric chromatin is remodeled to maintain functionality following structural change. Similarly, neocentromeres displayed greater accessibility than their flanking pericentromeric regions (Fig. 5E, Supplemental Fig. S14C), suggesting that remodeled centromeres tended to adopt chromatin configurations similar to the canonical centromeric chromatin.

We further observed a general increase in chromatin accessibility within (peri)centromeric regions of ditelosomic lines compared to CS wheat (Fig. 5D-E). In total, 465 differentially accessible chromatin regions (DARs) were identified, of which 441 were localized in pericentromeres (Fig. 6A and Supplemental Table S4). Most DARs were upregulated in ditelosomic lines and showed significantly greater fold changes in accessibility compared to downregulated DARs, and these DARs were enriched near genes, particularly in promoter

regions (Fig. 6B-C). These results suggest that enhanced chromatin openness may facilitate transcriptional activation and the deposition of CENH3 at the broken centromeres, consistent with the detection of novel transcripts associated with the upregulated DARs (Fig. 6D). Our findings suggest that centromeres stabilization following breakage may be accompanied by coordinated local changes in chromatin dynamics and transcription activation, consistent with previous reports showing that such changes prevent chromosomal translocations and preserve centromeric integrity in mammalian cells (Yilmaz et al. 2021; Li et al. 2023).

Discussion

Centromeres, characterized by their high content of repetitive DNAs, are pivotal in maintaining chromosome integrity. However, their repetitive nature renders them particularly fragile and prone to breakage, potentially leading to chromosomal translocations or nested insertions during evolutionary process (Hofstatter et al. 2022; Gambogi CW et al. 2023; Saayman et al. 2023). Despite their importance, the dynamic reorganization of centromere architecture following breakage and how this ensures faithful transmission of damaged chromosomes remains poorly understood. Previously studies have revealed that centromere breakage is regulated through the interplay of topological constraints, recombination, transcription, and replication (Li and Zhu 2022). Here, we delved into the molecular consequences of centromere breakage in wheat utilizing ditelosomic stocks (Gill et al. 1999). Our studies revealed localized chromosomal fragmentation and shattering near centromere break sites following breakages and subsequent generations, accompanied by centromere remodeling or even *de novo* centromere formation and telomere capture (Fig. 6E,

chromosomal level). These rearrangements, often involving terminal fragment duplications and interstitial deletions, are reminiscent of break-induced replication model (BIR) or BFB cycle. In maize, centromere formation and disappearance have been observed to occur rapidly, within as little as one or a few cell cycles after chromosomal rearrangements (Liu et al. 2020). Similarly, our results suggest that structural variations at breakpoints are most likely initiated within a few generations after breaks.

We show that wheat chromosomes may heal through *de novo* telomere capping and restoring centromere functionality to maintain karyotype stability (Fig. 6E). Alternatively, the capture of existing telomeric sequences could also account for these observation. Given the nature of the observed chromosomal rearrangements, *de novo* telomere addition remains a plausible and frequently reported mechanism for stabilizing these broken ends (McClintock 1939; McClintock 1941; Putnam et al. 2004; Ouenzar et al. 2017; Tan et al. 2024). Recent studies in engineering maize chromosome have shown that broken chromosome ends can be rapidly stabilized through *de novo* telomere formation (Zeng et al. 2025). Telomeres at the ends of chromosome arms are preserved by telomerase, which extends the 3’ overhang using species-specific repeats (Blackburn et al. 2015; Ouenzar et al. 2017). Although the mechanisms remain incompletely understood, in vitro studies have shown that telomerase can extend telomeric repeats from a variety of DNA templets (Fitzgerald et al. 2001; Margalef et al. 2018).

Centromere identity is epigenetically determined by the deposition of the histone variant CENH3, which recruits kinetochore proteins (Zhou et al. 2022). Our analysis revealed that centromere breakage in wheat leads to telosomes exhibiting varying degrees of centromere

integrity. The proximity of centromeres and telomeres in telosomic chromosomes requires spatial and temporal regulation to prevent functional interference. Our observations suggest that damaged centromeres possess a remarkable capacity for self-regulation through structural modifications such as expansion, shrinkage or neocentromere formation (Fig. 3-4). Following breakage, centromeres often undergo size changes before stabilizing at an “optimal size”. The optimal centromere size scales with chromosome size, as larger chromosomes require more microtubule attachments, necessitating larger kinetochores (Iwata-Otsubo et al. 2017). Instances of centromere contraction are relatively rare, implying that even reduced centromeres retain sufficient function for chromosome transmission (Watanabe 2012).

The precise repair and healing mechanisms following centromere misdivision enable the persistence of cells harboring chromosome fragments. Studies using CRISPR-Cas9-induced centromeric DSBs in mammalian cells have shown activation of either homologous recombination (HR) or non-homologous end joining (NHEJ) pathways (Tsouroula et al. 2016; Saayman et al. 2023). DNA-end resection, facilitated by the formation of DNA–RNA hybrids (R-loops) and increased H3K4me2-mediated transcription, helps initiate HR and prevents chromosomal translocations (Yilmaz et al. 2021). In our study, we also observed increased chromatin accessibility and elevated transcriptional activity near centromere breakpoints (Fig. 6E, chromatin level), which likely supports both the preservation of centromere function and structural remodeling. These results illustrate how centromere evolution is driven by the interplay of DNA repair, transcriptional regulation, and epigenetic reprogramming (Graham and Esashi 2024), and enhance our understanding of the structural and functional plasticity of centromeres in response to genomic stress. Due to the complexity of the wheat allohexaploid

354 genome and the limited depth of resequencing, it's currently not possible to precisely pinpoint
355 breakpoint locations. We also acknowledge this limitations of using short-read sequencing for
356 structural analyses, particularly when resolving centromeric regions. The large size and highly
357 repetitive nature of wheat centromeres present significant obstacles to achieve complete
358 genome assemblies for ditelosomic lines. Future studies employing long-read sequencing and
359 *de novo* assembly of the CSDt lines will be essential to fully resolving centromere breakage
360 events and reconstruction chromosome ends.
361
362 **Methods**
363 **Plant Materials**
364 The ditelosomic lines of the Chinese Spring wheat (CSDt) used in this study were generously
365 provided by Prof. Dengcai Liu from Sichuan Agricultural University, Prof. Hao Li from
366 Henan University, and Prof. Wanquan Ji from Northwest Agriculture and Forestry University.
367 Wheat seeds were germinated at room temperature and the plants were then transferred to soil
368 and grown in a greenhouse at 20°C with a 16-hour light and 8-hour dark photoperiod for two
369 weeks.
370
371 **Slide preparation and Fluorescence *in situ* hybridization (FISH) analysis**
372 For chromosome preparations, seeds were initially sprouted at room temperature in petri
373 dishes on moist filter paper. Treatment of root tips and FISH experiments were conducted
374 following the previously described protocol (Su et al. 2017). Wheat centromere repeat
375 sequences (CRW), telomere repeat sequence (Telomere), karyotype tandem repeats (pTa535-1

and pSc119.2) were utilized for non-denaturing FISH assays (Guo et al. 2016). These probes are effective at detecting regions with moderate to high copy numbers of tandem repeats (Komuro et al. 2013; Tang et al. 2014; Han et al. 2022). Genomic DNAs of *Triticum urartu* (AA, 2n=14), *Aegilops tauschii* (DD, 2n=14) and *Ae. speltoides* (BB, 2n=14) were employed for multi-color FISH (Huang et al. 2023). Fluorescence intensity of centromeres (two telocentric chromosomes and other intact chromosomes) from the long-arm ditelosomes were analyzed using ImageJ (v1.50i) as described previously (Guo et al. 2016). Integrated density values were averaged per nucleus from ~ 20 cells per line. Statistical difference was indicated by **, representing significant differences at $P < 0.01$ (Student's *t*-test).

Wheat whole-genome resequencing and data analysis

Genomic DNA was extracted from the leaves of wheat ditelosomic lines using the Plant DNA extraction kit (TIANGEN #DP304-03, Beijing, China). Libraries were constructed and sequenced on the MGI DNBSEQ-T7 high-throughput sequencing platform with 150 bp paired-end reads at Huazhong Agricultural University. To ensure data quality, low-quality reads and adapters were removed using fastp (v0.20.1) (Chen et al. 2018). The cleaned reads were aligned to the near gap-free reference genome of CS (Liu et al. 2025; Wang et al. 2025) using BWA-MEM (v0.7.17) with default parameters (Li and Durbin 2009). Genomic data visualization was facilitated using the Integrative Genomics Viewer (IGV, v2.102) (Thorvaldsdottir et al. 2013). We incorporated publicly available high-coverage re-sequencing data (~100.5×) for the same ditelosomic wheat lines (Accession NO. SRR10766573) ((IWGSC) 2014).

RNA-seq, data analysis, and Quantitative RT–PCR

Total RNA was extracted from the coleoptiles of wheat CS and ditelosomic lines using TRIzol reagent (Thermo Fisher, #15596018). Each sample included two biological replicates. 150-bp paired-end reads were generated on the Illumina NovaSeq 6000 platform. The clean data were first aligned to CS reference genome using STAR (v2.7.9a) (Dobin et al. 2013). Differential expression analysis was performed using the R package DESeq2 (v1.36.0), with criteria set for significant changes at a $\log_2$ (fold change) ≥ 1 and a FDR ≤ 0.05 (Love et al. 2014). Differentially expressed genes (DEGs) from each line were randomly selected for confirmation through Quantitative RT-PCR, and all primers detailed was listed in Supplemental Table S2.

Chromosomal structural and segment copy number variations analysis

Mapping files were processed using mosdepth software to assess whole genome sequencing coverage within 100-kb windows (Pedersen and Quinlan 2018). Subsequently, copy number variations (CNVs) were validated using the CNVnator tool (Abyzov et al. 2011). Primers were meticulously designed to specifically target the regions of copy number variation in the wheat ditelosomic lines (Supplemental Table S2). Centromeric regions were divided into consecutive 1-kb non-overlapping windows, and putative breakpoint-associated regions were identified based on abrupt changes in sequencing coverage. Chromosomal deletion regions were operationally defined as contiguous genomic segments in which at least seven consecutive windows showed coverage of fewer than five reads per window.

Breakpoint-associated regions were defined and manually checked as the first window of a deletion region together with its immediately adjacent non-deletion window (Supplemental Table S1).

Chromatin immunoprecipitation assays with sequencing and ChIP-seq analysis

Wheat ditelosomic lines were subjected to ChIP-seq experiments following established protocols with minor adjustments (Liu et al. 2015). The process included the cell nuclei extraction, chromatin fragmentation, and immunoprecipitation using specific antibodies. Wheat-specific CENH3 (Su et al. 2019) and commercially available H3K9me2 antibodies (Abcam, #ab1220) were utilized for the ChIP-seq experiments. ChIP-seq data pre-analysis mirrored the approach for genomic resequencing and the whole-genome resequencing data from the same ditelosomic lines were used as controls. CENH3 nucleosomes midpoint positions on wheat CRW retrotransposons and dinucleotide patterns around CENH3 nucleosomes were examined following previous method (Su et al. 2019).

ATAC-seq library construction, sequencing and data analysis

ATAC-seq experiments on wheat lines from the coleoptiles were conducted using established methodologies (Wang et al. 2022). Libraries were then purified, and sequenced on the Illumina NovaSeq 6000 system, generating 150-bp paired-end reads. ATAC-seq data analysis was executed using the wheatATAC pipeline (https://github.com/hcph/wheatATAC.git). The quality of the ATAC-seq data was assessed by analyzing library insert fragments, library complexity, and the consistency between sample replicates using the Irreproducibility

Discovery Rate (IDR). The Fraction of Reads in Peaks (FRiP) was calculated to determine the percentage of reads within peaks relative to total reads. The distribution of reads in the centromere and pericentromere were assessed using corresponding windows, respectively.

Calculation of DNA methylation level

DNA methylation data for the CS line was retrieved from the NCBI database under accession number SRP133674 (Ramirez-Gonzalez et al. 2018). The filter reads were aligned to the reference genome using Bismark (v0.24.1) with parameters "-bowtie 2 -N 1 -L 20" (Krueger and Andrews 2011). Methylation ratios were calculated by dividing the number of methylated cytosines (mCs) at a position by the total number of reads covering that position. Only positions with more than 3 reads were considered plausible methylation loci for subsequent analyses.

Data access

The WGS-seq, RNA-seq, and ATAC-seq data in this study have been submitted to the Genome Sequence Archive (GSA) database in the NGDC (https://ngdc.cncb.ac.cn/) under accession numbers CRA018693 and CRA018696.

Software availability

The code used for data analysis is freely accessible at GitHub (https://github.com/Jwzhou0402/ditelosomic) and as Supplemental Scripts.

Competing interest statement

The authors declare no competing interests.

Acknowledgements

We thank Nathan D. Han from The Edison Family Center for critical reading of the article and helpful comments, and the high-performance computing platform at National Key Laboratory of Crop Genetic Improvement in Huazhong Agricultural University. This project was financially supported by the National Key Research and Development Program of China (2021YFF1000800), and the National Natural Science Foundation of China (32170571 and 32400451). Project 2662024JC010 supported by the Fundamental Research Funds for the Central Universities. Additional funding was provided by the Young Top-notch Talent Cultivation Program of Hubei Province and the Natural Science Foundation of Hubei Province of China (2024AFB116).

Author contributions: H.D.S. designed the research; J.W.Z., Y.H.H., H.M., Q.Y.C., C.Y.C., performed research; J.W.Z., Y.H.H., and H.D.S. analyzed data; H.D.S. wrote the article.

Reference

(IWGSC) IWGSC. 2014. A chromosome-based draft sequence of the hexaploid bread wheat (Triticum aestivum) genome. *Science* **345**: 1251788.

Abyzov A, Urban AE, Snyder M, Gerstein M. 2011. CNVnator: an approach to discover, genotype, and characterize typical and atypical CNVs from family and population genome sequencing. *Genome Res* **21**: 974-984.

Bakhoum SF, Cantley LC. 2018. The Multifaceted Role of Chromosomal Instability in Cancer and Its Microenvironment. *Cell* **174**: 1347-1360.

Barra V, Fachinetti D. 2018. The dark side of centromeres: types, causes and consequences of structural abnormalities implicating centromeric DNA. *Nat Commun* **9**: 4340.

Birchler JA, Han FP. 2018. Barbara McClintock's Unsolved Chromosomal Mysteries: Parallels to Common Rearrangements and Karyotype Evolution. *Plant Cell* **30**: 771-779.

Blackburn EH, Epel ES, Lin J. 2015. Human telomere biology A contributory and interactive factor in aging, disease risks, and protection. *Science* **350**: 1193-1199.

Bloom K. 2024. Chromosome segregation: Brushing up on centromeres. *Curr Biol* **34**: R565-R567.

Bosco N, Goldberg A, Zhao X, Mays JC, Cheng P, Johnson AF, Bianchi JJ, Toscani C, Di Tommaso E, Katsnelson L et al. 2023. KaryoCreate: A CRISPR-based technology to study chromosome-specific aneuploidy by targeting human centromeres. *Cell* **186**: 1985-2001 e1919.

Chen C, Wu S, Sun Y, Zhou J, Chen Y, Zhang J, Birchler JA, Han F, Yang N, Su H. 2024. Three near-complete genome assemblies reveal substantial centromere dynamics from diploid to tetraploid in Brachypodium genus. *Genome Biol* **25**: 63.

Chen S, Zhou Y, Chen Y, Gu J. 2018. fastp: an ultra-fast all-in-one FASTQ preprocessor. *Bioinformatics* **34**: i884-i890.

Chmatal L, Gabriel SI, Mitsainas GP, Martinez-Vargas J, Ventura J, Searle JB, Schultz RM, Lampson MA. 2014. Centromere strength provides the cell biological basis for meiotic drive and karyotype evolution in mice. *Curr Biol* **24**: 2295-2300.

Darlington CD. 1939. Misdivision and the genetics of the centromere. *J Genet* **37**: 341-364.

Devos KM, Sorrells ME, Anderson JA, Miller TE, Reader SM, Lukaszewski AJ, Dubcovsky J,

Sharp PJ, Faris J, Gale MD. 1999. Chromosome aberrations in wheat nullisomic-tetrasomic and ditelosomic lines. *Cereal Res Commun* **27**: 231-239.

Dobin A, Davis CA, Schlesinger F, Drenkow J, Zaleski C, Jha S, Batut P, Chaisson M, Gingeras TR. 2013. STAR: ultrafast universal RNA-seq aligner. *Bioinformatics* **29**: 15-21.

Fitzgerald MS, Shakirov EV, Hood EE, McKnight TD, Shippen DE. 2001. Different modes of de novo telomere formation by plant telomerases. *Plant J* **26**: 77-87.

Gambogi CW, Pandey N, Dawicki-McKenna JM, Arora UP, Liskovykh MA, Ma J, Lamelza P, Larionov V, Lampson MA, Logsdon GA et al. 2023. Centromere innovations within a mouse species. *Sci Adv* **9**: eadi5764.

Gill KS, Arumuganathan K, Lee JH. 1999. Isolating individual wheat (Triticum aestivum) chromosome arms by flow cytometric analysis of ditelosomic lines. *Theor Appl Genet* **98**: 1248-1252.

Graham E, Esashi F. 2024. DNA strand breaks at centromeres: Friend or foe? *Seminars Cell Dev Biol* **156**: 141-151.

Guo X, Su H, Shi Q, Fu S, Wang J, Zhang X, Hu Z, Han F. 2016. De Novo Centromere Formation and Centromeric Sequence Expansion in Wheat and its Wide Hybrids. *PLoS Genet* **12**: e1005997.

Han G, Yan H, Wang J, Cao L, Liu S, Li X, Zhou Y, Fan J, Li L, An D. 2022. Molecular Cytogenetic Identification of a New Wheat-Rye 6R Addition Line and Physical Localization of Its Powdery Mildew Resistance Gene. *Front Plant Sci* **13**: 889494.

Hofstatter PG, Thangavel G, Lux T, Neumann P, Vondrak T, Novak P, Zhang M, Costa L,

Castellani M, Scott A et al. 2022. Repeat-based holocentromeres influence genome architecture and karyotype evolution. *Cell* **185**: 3153-3168.e3118.

Huang Y, Shi Q, Zhou C, Wang C, Liu Y, Yi C, Su H, Han F. 2023. Wide hybridizations reveal the robustness of functional centromeres in Triticum-Aegilops species complex lines. *J Genet Genomics* **51**: 570-573.

Iwata-Otsubo A, Dawicki-McKenna JM, Akera T, Falk SJ, Chmatal L, Yang K, Sullivan BA, Schultz RM, Lampson MA, Black BE. 2017. Expanded Satellite Repeats Amplify a Discrete CENP-A Nucleosome Assembly Site on Chromosomes that Drive in Female Meiosis. *Curr Biol* **27**: 2365-2373 e2368.

Kiesselbach TA. 1949. The structure and reproduction of corn. *University of Nebraska Agricultural Experiment Station, Res Bulletin* **161**.

Kim E, Kim J, Kim C, Lee J. 2021. Long-read sequencing and de novo genome assemblies reveal complex chromosome end structures caused by telomere dysfunction at the single nucleotide level. *Nucleic Acids Res* **49**: 3338-3353.

Kolbin D, Locatelli M, Stanton J, Kesselman K, Kokkanti A, Li J, Yeh E, Bloom K. 2025. Centromeres are stress-induced fragile sites. *Curr Biol* **35**: 1197-1210.e1194.

Komuro S, Endo R, Shikata K, Kato A. 2013. Genomic and chromosomal distribution patterns of various repeated DNA sequences in wheat revealed by a fluorescence in situ hybridization procedure. *Genome* **56**: 131-137.

Koo D-H, Sehgal SK, Friebe B, Gill BS. 2015. Structure and Stability of Telocentric Chromosomes in Wheat. *PloS One* **10**: e0137747.

Kopecky D, Lukaszewski AJ. 2019. Misdivision of Telocentrics and Isochromosomes in Wheat.

Cytogenetic Genome Res **157**: 179-188.

Krueger F, Andrews SR. 2011. Bismark: a flexible aligner and methylation caller for Bisulfite-Seq applications. *Bioinformatics* **27**: 1571-1572.

Levy AA, Feldman M. 2022. Evolution and origin of bread wheat. *The Plant Cell* **34**: 2549-2567.

Li H, Durbin R. 2009. Fast and accurate short read alignment with Burrows-Wheeler transform. *Bioinformatics* **25**: 1754-1760.

Li JSZ, Abbasi A, Kim DH, Lippman SM, Alexandrov LB, Cleveland DW. 2023. Chromosomal fragile site breakage by EBV-encoded EBNA1 at clustered repeats. *Nature* **616**: 504-509.

Li R, Zhu J. 2022. Effects of aneuploidy on cell behaviour and function. *Nat Rev Mol Cell Biol* **23**: 250-265.

Liu S, Li K, Dai X, Qin G, Lu D, Gao Z, Li X, Song B, Bian J, Ren D et al. 2025. A telomere-to-telomere genome assembly coupled with multi-omic data provides insights into the evolution of hexaploid bread wheat. *Nat Genet* **57**: 1008-1020.

Liu Y, Su H, Pang J, Gao Z, Wang XJ, Birchler JA, Han F. 2015. Sequential de novo centromere formation and inactivation on a chromosomal fragment in maize. *Proc Natl Acad Sci U S A* **112**: E1263-1271.

Liu Y, Su H, Zhang J, Shi L, Liu Y, Zhang B, Bai H, Liang S, Gao Z, Birchler JA et al. 2020. Rapid Birth or Death of Centromeres on Fragmented Chromosomes in Maize. *Plant Cell* **32**: 3113-3123.

Love MI, Huber W, Anders S. 2014. Moderated estimation of fold change and dispersion for

RNA-seq data with DESeq2. *Genome Biol* **15**: 550.

Lu M, He X. 2019. Centromere repositioning causes inversion of meiosis and generates a reproductive barrier. *Proc Natl Acad Sci U S A* **116**: 21580-21591.

Lukaszewski AJ. 2010. Behavior of centromeres in univalents and centric misdivision in wheat. *Cytogenet Genome Res* **129**: 97-109.

Lysak MA. 2022. Celebrating Mendel, McClintock, and Darlington: On end-to-end chromosome fusions and nested chromosome fusions. *Plant Cell* **34**: 2475-2491.

Mandakova T, Hlouskova P, Koch MA, Lysak MA. 2020. Genome Evolution in Arabideae Was Marked by Frequent Centromere Repositioning. *Plant Cell* **32**: 650-665.

Margalef P, Kotsantis P, Borel V, Bellelli R, Panier S, Boulton SJ. 2018. Stabilization of Reversed Replication Forks by Telomerase Drives Telomere Catastrophe. *Cell* **172**: 439-453.e414.

McClintock B. 1939. The Behavior in Successive Nuclear Divisions of a Chromosome Broken at Meiosis. *Proc Natl Acad Sci U S A* **25**: 405-416.

McClintock B. 1941. The stability of broken ends of chromosomes in zea mays. *Genetics* **26**: 234-282.

Ouenzar F, Lalonde M, Laprade H, Morin G, Gallardo F, Tremblay-Belzile S, Chartrand P. 2017. Cell cycle-dependent spatial segregation of telomerase from sites of DNA damage. *J Cell Biol* **216**: 2355-2371.

Pedersen BS, Quinlan AR. 2018. Mosdepth: quick coverage calculation for genomes and exomes. *Bioinformatics* **34**: 867-868.

Pentzold C, Kokal M, Pentzold S, Weise A. 2021. Sites of chromosomal instability in the

context of nuclear architecture and function. *Cell Mol Life Sci* **78**: 2095-2103.

Putnam CD, Pennaneach V, Kolodner RD. 2004. Chromosome healing through terminal deletions generated by de novo telomere additions in Saccharomyces cerevisiae. *Proc Natl Acad Sci U S A* **101**: 13262-13267.

Ramirez-Gonzalez RH, Borrill P, Lang D, Harrington SA, Brinton J, Venturini L, Davey M, Jacobs J, van Ex F, Pasha A et al. 2018. The transcriptional landscape of polyploid wheat. *Science* **361**: eaar6089.

Saayman X, Graham E, Nathan WJ, Nussenzweig A, Esashi F. 2023. Centromeres as universal hotspots of DNA breakage, driving RAD51-mediated recombination during quiescence. *Mol Cell* **83**: 523-538 e527.

Sears ER. 1954. The Aneuploids of Common Wheat. *Research Bulletin, Missouri Agricultural Experiment Station* **572**: 1-58.

Showman S, Talbert PB, Xu Y, Adeyemi RO, Henikoff S. 2024. Expansion of human centromeric arrays in cells undergoing break-induced replication. *Cell Rep* **43**: 113851.

Su H, Liu Y, Dong Q, Feng C, Zhang J, Liu Y, Birchler JA, Han F. 2017. Dynamic location changes of Bub1-phosphorylated-H2AThr133 with CENH3 nucleosome in maize centromeric regions. *New Phytol* **214**: 682-694.

Su H, Liu Y, Liu C, Shi Q, Huang Y, Han F. 2019. Centromere Satellite Repeats Have Undergone Rapid Changes in Polyploid Wheat Subgenomes. *Plant Cell* **31**: 2035-2051.

Tan K-T, Slevin MK, Leibowitz ML, Garrity-Janger M, Shan J, Li H, Meyerson M. 2024.

Neotelomeres and telomere-spanning chromosomal arm fusions in cancer genomes revealed by long-read sequencing. *Cell Genomics* **4**: 100588.

Tang Z, Yang Z, Fu S. 2014. Oligonucleotides replacing the roles of repetitive sequences pAs1, pSc119.2, pTa-535, pTa71, CCS1, and pAWRC.1 for FISH analysis. *J Appl Genet* **55**: 313-318.

Thorvaldsdottir H, Robinson JT, Mesirov JP. 2013. Integrative Genomics Viewer (IGV): high-performance genomics data visualization and exploration. *Brief Bioinformatics* **14**: 178-192.

Tsouroula K, Furst A, Rogier M, Heyer V, Maglott-Roth A, Ferrand A, Reina-San-Martin B, Soutoglou E. 2016. Temporal and Spatial Uncoupling of DNA Double Strand Break Repair Pathways within Mammalian Heterochromatin. *Mol Cell* **63**: 293-305.

Wang X, Chen C, He C, Chen D, Yan W. 2022. Mapping open chromatin by ATAC-seq in bread wheat. *Front Plant Sci* **13**: 1074873.

Wang Z, Miao L, Tan K, Guo W, Xin B, Appels R, Jia J, Lai J, Lu F, Ni Z et al. 2025. Near-complete assembly and comprehensive annotation of the wheat Chinese Spring genome. *Mol Plant* doi:10.1016/j.molp.2025.02.002.

Watanabe Y. 2012. Geometry and force behind kinetochore orientation: lessons from meiosis. *Nat Rev Mol Cell Biol* **13**: 370-382.

Willson J. 2020. Resolving the roles of structural variants. *Nat Rev Genet* **21**: 507.

Yadav V, Sun S, Coelho MA, Heitman J. 2020. Centromere scission drives chromosome shuffling and reproductive isolation. *Proc Natl Acad Sci U S A* **117**: 7917-7928.

Yilmaz D, Furst A, Meaburn K, Lezaja A, Wen Y, Altmeyer M, Reina-San-Martin B, Soutoglou

E. 2021. Activation of homologous recombination in G1 preserves centromeric integrity. *Nature* **600**: 748-753.

Zagelbaum J, Schooley A, Zhao J, Schrank BR, Callen E, Zha S, Gottesman ME, Nussenzweig A, Rabadan R, Dekker J et al. 2023. Multiscale reorganization of the genome following DNA damage facilitates chromosome translocations via nuclear actin polymerization. *Nat Structural Mol Biol* **30**: 99-106.

Zeng Y, Wang M, Jonathan IG, R. Kelly D. 2025. Increased maize chromosome number by engineered chromosome fission. *Sci Adv* **11**: eadw3433.

Zhou J, Liu Y, Guo X, Birchler JA, Han F, Su H. 2022. Centromeres: from chromosome biology to biotechnology applications and synthetic genomes in plants. *Plant Biotechnol J* **20**: 2051-2063.

Fig Legends

Fig 1. Distribution of centromere and telomere signals on ditelosomic and corresponding chromosomes in Chinese Spring (CS) wheat.

(A) Fluorescence *in situ* hybridization (FISH) analysis illustrates centromere and telomere distribution on ditelosomic chromosomes derived from homoeologous groups 1, 6, and 7, as well as on their corresponding full-length chromosomes in Chinese Spring (CS) wheat. Chromosomal DNA is counterstained with 4',6-Diamidino-2-phenylindole (DAPI, blue). Centromeres are labeled in red using the centromere-specific probe CCS1, and telomeres are labeled in green using a telomere-specific probe. Each panel displays the short arm (S) and long arm (L) telosomes from A, B, and D genomes, along with the full chromosomes

(Chr1A-Chr1D, Chr6A-Chr7D), clearly showing variations in centromere and telomere positioning and signaling. Scale bar is 10 μm. (B) Fluorescence intensity of CRW fluorescence in long-arm ditelosomic lines. Centromeric signals from two telocentric chromosomes were compared with those from other intact chromosomes for each line. The Y-axis indicates relative CRW fluorescence intensity, with error bars representing standard deviation (s.d.). ** denote significant differences at $P < 0.01$ (Student's *t*-test). (C) A schematic model illustrating centromere misdivision-induced chromosome breakage in wheat. Three scenarios of centromere breakage are depicted: breakage within centromere (internal), on one side, or on both sides of the centromere. Chromosome healing is hypothesized to occur through the *de novo* addition of telomeric repeats at the breakpoint ends. Chromosome arms are shown in blue, centromeres in red, and telomeres in green.

Fig 2. Localized complex chromosomal structural variations at damaged centromeres in wheat ditelosomic lines.

(A-C) Genomic-wide resequencing read depth analysis around centromere breakpoints in ditelosomic chromosomes from wheat homologous groups 1 (A), 6 (B), and 7 (C). Each subpanel displays multiple tracks: the top track marks the centromeric regions based on CENH3 ChIP-seq signals. The next four tracks show normalized resequencing coverage (Reads Per Genomic Content, RPGC) in 10-bp bins for Chinese Spring (CS) wheat and both short-arm (S) and long-arm (L) telosomes of ditelosomic lines. The bottom track presents annotated gene distributions. Triangles in the CS tracks denote primer positions used for PCR validation of genomic regions near breakpoints. (D) Agarose gel electrophoresis results

showing the presence (red) or deletion (blue) of specific terminal chromosomal fragments in various ditelosomic lines. PCR amplifications were conducted using primers targeting regions flanking the breakpoints in Chromosome 1, 6, and 7. (E) Copy number variations (CNVs) in genomic regions adjacent to breakpoints, based on read depth analysis. Four specific intervals are shown: Dt1AL (Chr1A: 216,799,654–217,769,250), Dt1BS (Chr1B: 243,980,001–245,644,800), Dt6AL (Chr6A: 293,023,801–293,313,400), and Dt7AL (Chr7A: 362,003,351–362,687,599). Each line shows altered read depth, reflecting structural rearrangements and CNVs. (F) Quantitative PCR (qPCR) analysis validating the CNVs observed in panel (E). Relative copy number values for targeted genomic fragments are shown for ditelosomic lines and compared against CS wheat. Statistical significance was assessed using Student's *t*-tests; $P \leq 0.01$ is indicated by **.

Fig 3. Remodeling of centromere architecture is associated with local structural variations and centromere repositioning following misdivision in wheat ditelosomic lines. (A-C) Comparative analysis of CENH3-enriched centromere domains between Chinese Spring (CS) wheat and specific ditelosomic lines: Dt7DS and Dt7DL (A), Dt6BL (B), and Dt1BL (C). Integrated Genomics Viewer (IGV) snapshots display CENH3 ChIP-seq enrichment patterns, genomic DNA coverage, and gene annotations across defined centromeric regions. In Dt7DS and Dt7DL, centromere structure and CENH3 positioning remain stable, consistent with the CS reference. In Dt6BL, a contraction of the CENH3-enriched domain is observed, indicating centromere shrinkage. In contrast, Dt1BL shows expansion of the centromere region. Correlation coefficients (R-values) quantify the

similarity of CENH3 nucleosome positioning between ditelosomic chromosomes and their CS counterparts, calculated within the shared centromere intervals (highlighted in grey rectangles). (D) Boxplot showing the correlation of CENH3 nucleosome distributions across chromosome. Top panel indicate the overall correlation between ditelosomic chromosomes (with centromere breakage) and other unaltered chromosomes compared to CS. Bottom panel indicate comparison of correlation in regions with local structural variations (SV region) versus those without (non-SV region), suggesting that centromere remodeling is not predominantly driven by surrounding chromosomal rearrangements. (E) Dinucleotide frequency analysis within ±200 bp flanking CENH3 nucleosome centers reveals conserved sequence features between ditelosomic and their corresponding chromosomes in CS. Peaks in WW (A or T) and SS (G or C) motifs are consistent across lines, indicating that underlying sequence composition near CENH3 remains largely unchanged. (F) Metaprofile analysis of CENH3 signals distribution around centromeric retrotransposon repeat of wheat (CRW) compares ditelosomic chromosomes to their full-length counterparts in CS (left). Pearson correlation coefficients and the number of CRWs analyzed (n=771) are shown (right), indicating conservation of centromeric chromatin structure at the retroelement level. Student's *t*-tests assess statistical differences in signal enrichment; $P < 0.05$ is indicated by *, while "ns" denotes non-significant differences.

Fig 4. *De novo* centromeres formation in acentric chromosome fragments following centromere deletion and complex structural rearrangements in wheat.

(A) Schematic model depicting centromere misdivision leading to the chromosome breakage

and the formation of a neocentromerein wheat. Breakage (indicated by arrowhead) occurs near one side of the original centromere, resulting in an acentric chromosome fragment. Subsequent local fragmentation and rearrangement lead to the deletion of the native centromere. A new CENH3-enriched domain is established at a novel chromosomal location, often adjacent to the former centromeric region, indicating neocentromere seeding. (B) CENH3 ChIP-seq signal profiles in the centromeric regions of Dt1BS (left), Dt6BS (middle), and Dt7AS (right), compared to their corresponding regions in CS wheat. Neocentromeres and their syntenic positions in CS are highlighted in gray. IGV snapshot showing DNA methylation levels (CG, CHG and CHH contexts), gene annotations, and genomic coordinates are shown below. CENH3 relocation indicates centromere repositioning relative to CS. (C) Quantitative comparison of gene and transposable element (TE) density across three genomic regions: the original centromere (CEN), the neocentromere (NeoCEN), and the flanking pericentromeric regions (PERI), calculated in 10-Mb windows. TE density is elevated in NeoCEN relative to surrounding regions, while gene density shows moderate variation. (D) Gene expression levels and corresponding CENH3 enrichment are shown for 23 annotated genes (G1 to G23) located within and around the neocentromeric region. Expression values across six wheat tissues (root, coleoptile, stem, leaf, spike, and grain) are provided. CENH3 enrichment is plotted separately, indicating localized centromeric chromatin reestablishment over a subset of these genes. (E) Whole-genome bisulfite sequencing (WGBS) analysis reveals DNA methylation levels (CG, CHG, CHH contexts) in CS wheat across the CEN, NeoCEN, and PERI regions. NeoCEN and PERI regions in CS background show different methylation profiles relative to native centromeres. Statistical significance was assessed using

752 Student's *t*-test. P < 0.05 is indicated by *, P < 0.01 is indicated by **, while "ns" denotes
753 non-significant differences.
754
755 **Fig 5. Coordinated changes in gene expression and chromatin accessibility within**
756 **(peri)centromere regions in wheat ditelosomic lines.**
757 (A) Volcano plot showing differentially expressed genes (DEGs) within (peri)centromeric
758 regions in ditelosomic lines compared to CS wheat. Each point represents a gene; red and blue
759 dots denote significantly upregulated and downregulated genes, respectively, based on
760 RNA-seq data. The number of DEGs is indicated for each group. (B) Correlation analysis
761 between chromatin accessibility (measured by ATAC-seq) and gene expression (assessed by
762 RNA-seq) within (peri)centromeric regions. Top panel shows the overall correlation between
763 genes with significant expression changes and their accessibility changes. Bottom panels
764 display the distribution of open chromatin signals across transcription start sites (TSS) and
765 transcription end sites (TES), highlighting shifts in chromatin accessibility patterns.
766 Significantly upregulated and downregulated genes were displayed in left and right panels. (C)
767 IGV snapshots showing RNA-seq and ATAC-seq signal tracks across the centromeric and
768 pericentromeric regions of Dt7BL and CS wheat. Genes with significant expression changes
769 are highlighted: red and blue dots indicate up- and down-regulated genes, and gray dots
770 represent those with no significant change. Two example genes, *TraesCSC7B01G273700* and
771 *TraesCSC7B01G278100*, are displayed with enlarged views, showing CENH3 enrichment,
772 chromatin accessibility (ATAC-seq), and transcriptional activity (RNA-seq) between the
773 Dt7BL and CS wheat. (D) Comparative analysis of ATAC-seq signal changes between

774 centromeric (CEN) and pericentromereic (PERI) regions within CS and ditelosomic lines
775 under different centromere states, including maintenance, expansion, shrinkage, and
776 neocentromere formation. The schematic above indicates the specific regions compared in
777 each category, with highlighted regions corresponding to structural transitions. ATAC-seq
778 signal intensity is compared across CS and ditelosomic lines, and statistical significance is
779 evaluated using Student's *t*-test ($P < 0.05$ indicated by *, $P < 0.01$ by **, and "ns" = not
780 significant).
781
782 **Fig 6. Enhanced chromatin accessibility facilitates transcriptional activation and**
783 **promotes chromosome stability in damaged centromeres.**
784 (A) The number of differentially accessible chromatin regions (DARs) identified within
785 (peri)centromeric regions of ditelosomic lines compared to CS wheat, stratified by centromere
786 architecture types: neocentromere, contraction, expansion and maintenance. Red and green
787 bars represent upregulated (n=29) and downregulated (n=34) DARs, respectively. The number
788 of DARs is highest in upregulated, reflecting increased chromatin remodeling. (B)
789 Comparison of the absolute fold changes ($|\log_2 FC|$) between upregulated (red) and
790 downregulated (green) DARs. Upregulated DARs show significantly higher fold changes,
791 indicating more pronounced chromatin opening. Statistical significance is evaluated using
792 Student's *t*-test ($P < 0.01$ by **). (C) Genomic distribution of DARs across functional regions
793 within (peri)centromeric regions, including promoter (<=5 kb), 3' untranslated regions
794 (UTRs), exons, introns, downstream regions (<=300 bp), and distal intergenic regions.
795 Observed distributions of DARs are compared with expected background frequencies of these

various genomic regions, highlighting enrichment in promoter and intergenic areas. (D) Representative IGV snapshot of Dt1AL and Dt7DL lines compared to CS wheat, showing ATAC-seq (chromatin accessibility), RNA-seq (transcription activity), and CENH3 ChIP-seq signals within pericentromeric regions. DARs, novel transcripts, and TEs identified in ditelosomic lines are also indicated. The examples illustrate the emergence of open chromatin regions and transcriptional activation near restructured centromeres. (E) Schematic model illustrating how centromere damage initiates coordinated local changes in chromatin dynamics and transcriptional activation in wheat. Centromere breakage results in fragmental duplication, deletion, and in some cases a subset of these chromosomal fragmented pieces being randomly reassembled. This structural reorganization results in CENH3 nucleosome repositioning and neocentromere formations or altered centromere states. Concurrently, this process is coupled with localized, coordinated gene expression changes and open chromatin alterations that follow centromere misdivision, where enhanced chromatin openness promote transcriptional activation and may contribute to chromosome stability in the absence of an intact canonical centromere.

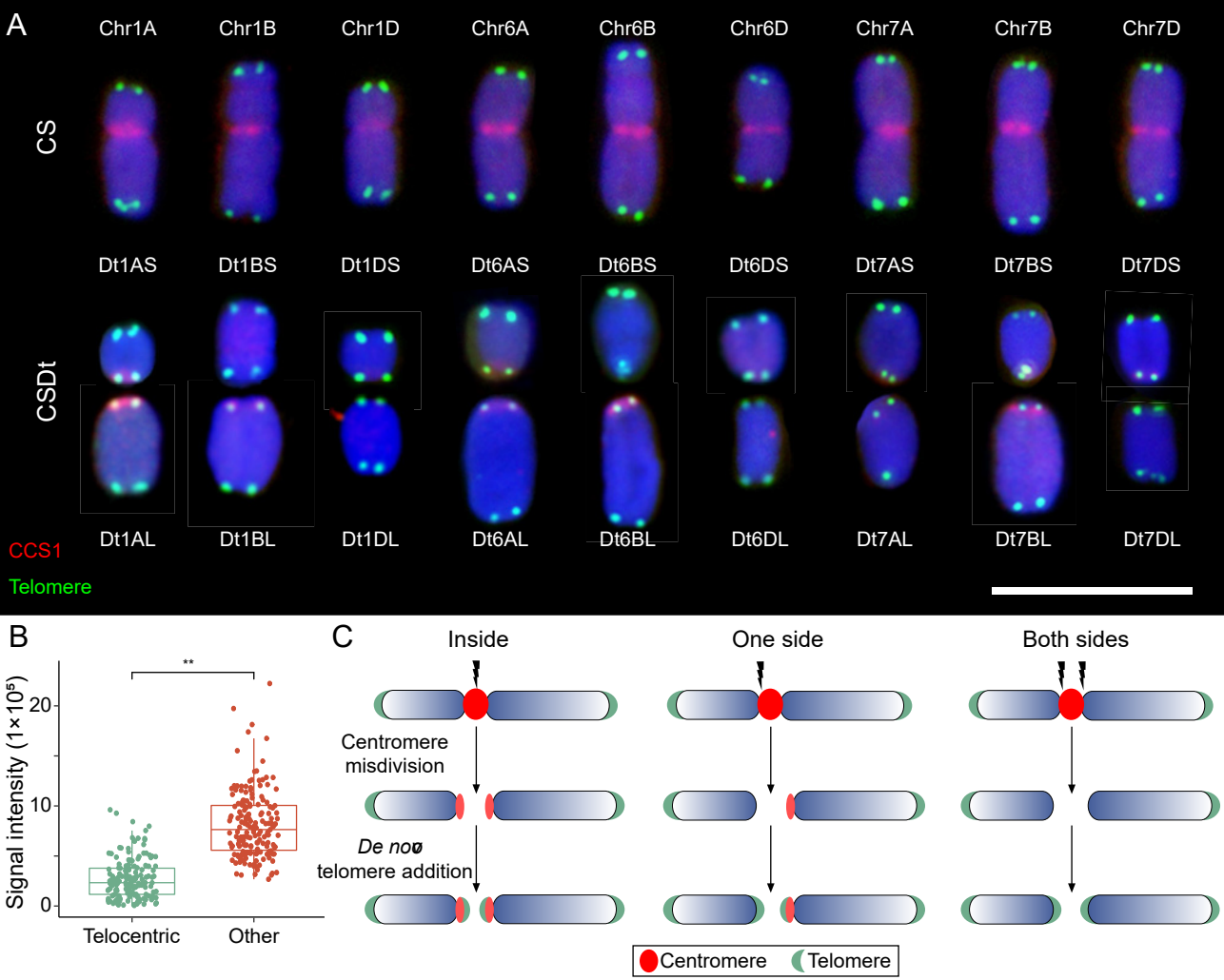
A
Chr1A
Chr1B
Chr1D
Chr6A
Chr6B
Chr6D
Chr7A
Chr7B
Chr7D
CS
Dt1AS
Dt1BS
Dt1DS
Dt6AS
Dt6BS
Dt6DS
Dt7AS
Dt7BS
Dt7DS
CSDt
Dt1AL
Dt1BL
Dt1DL
Dt6AL
Dt6BL
Dt6DL
Dt7AL
Dt7BL
Dt7DL
CCS1
Telomere
B
**
Signal intensity (1×10⁵)
20
10
0
Telocentric
Other
C
Inside
One side
Both sides
Centromere misdivision
De novo telomere addition
Centromere
Telomere

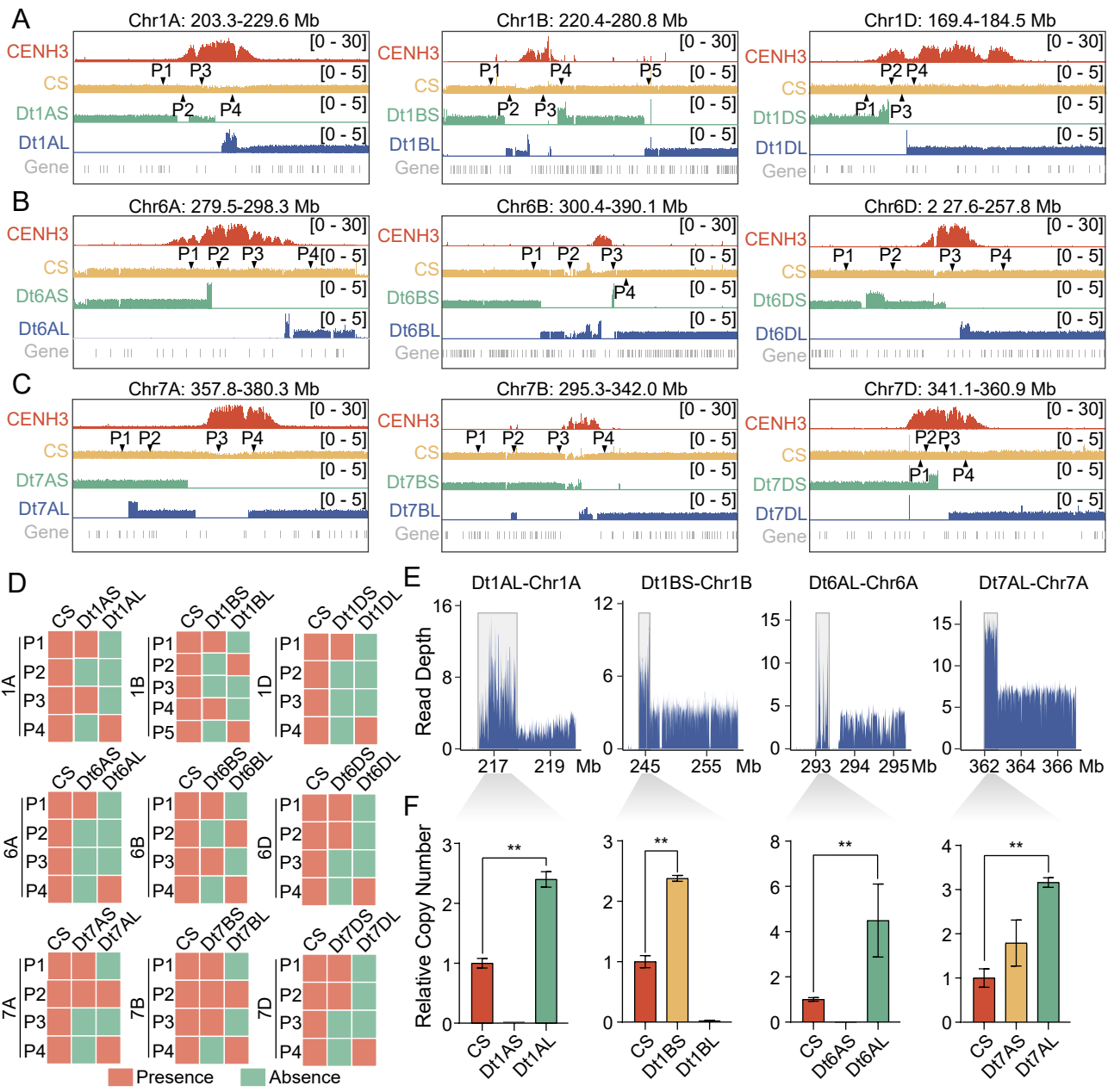
A
Chr1A: 203.3-229.6 Mb
Chr1B: 220.4-280.8 Mb
Chr1D: 169.4-184.5 Mb
CENH3
CS
Dt1AS
Dt1AL
Dt1BS
Dt1BL
Dt1DS
Dt1DL
Gene
[0 - 30]
[0 - 5]
P1
P2
P3
P4
P5
B
Chr6A: 279.5-298.3 Mb
Chr6B: 300.4-390.1 Mb
Chr6D: 2 27.6-257.8 Mb
Dt6AS
Dt6AL
Dt6BS
Dt6BL
Dt6DS
Dt6DL
C
Chr7A: 357.8-380.3 Mb
Chr7B: 295.3-342.0 Mb
Chr7D: 341.1-360.9 Mb
Dt7AS
Dt7AL
Dt7BS
Dt7BL
Dt7DS
Dt7DL
D
1A
1B
1D
6A
6B
6D
7A
7B
7D
Presence
Absence
E
Dt1AL-Chr1A
Dt1BS-Chr1B
Dt6AL-Chr6A
Dt7AL-Chr7A
Read Depth
Mb
F
Relative Copy Number
**

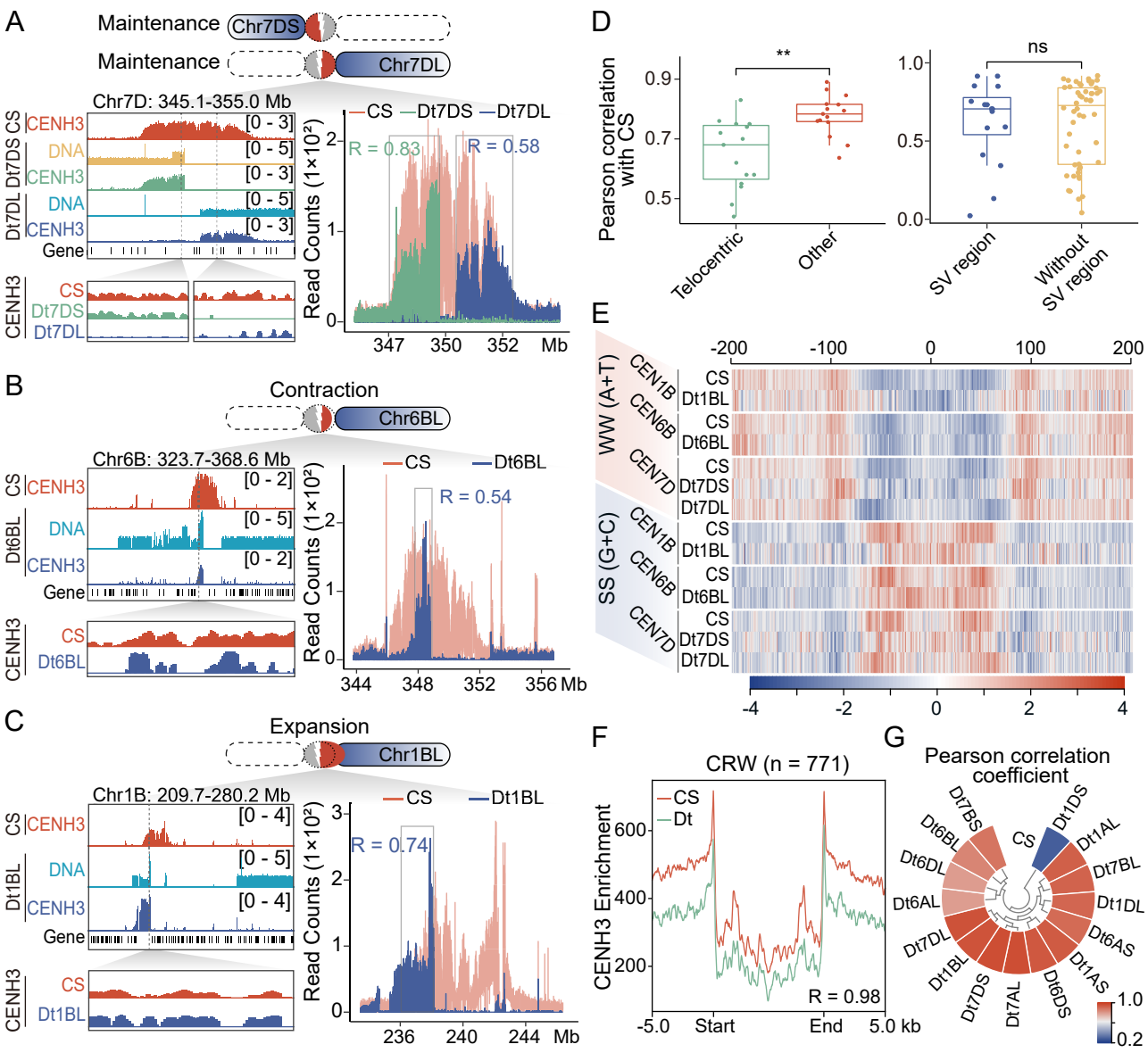
A
Maintenance
Chr7DS
Maintenance
Chr7DL
Chr7D: 345.1-355.0 Mb
CS
CENH3
[0 - 3]
DNA
[0 - 5]
Dt7DS
CENH3
[0 - 3]
DNA
[0 - 5]
Dt7DL
CENH3
[0 - 3]
Gene
CENH3
CS
Dt7DS
Dt7DL
CS
Dt7DS
Dt7DL
R = 0.83
R = 0.58
Read Counts (1×10²)
347
350
352
Mb
B
Contraction
Chr6BL
Chr6B: 323.7-368.6 Mb
CS
CENH3
[0 - 2]
DNA
[0 - 5]
Dt6BL
CENH3
[0 - 2]
Gene
CENH3
CS
Dt6BL
CS
Dt6BL
R = 0.54
Read Counts (1×10²)
344
348
352
356 Mb
C
Expansion
Chr1BL
Chr1B: 209.7-280.2 Mb
CS
CENH3
[0 - 4]
DNA
[0 - 5]
Dt1BL
CENH3
[0 - 4]
Gene
CENH3
CS
Dt1BL
CS
Dt1BL
R = 0.74
Read Counts (1×10²)
236
240
244
Mb
D
Pearson correlation with CS
**
ns
Telocentric
Other
SV region
Without SV region
E
WW (A+T)
SS (G+C)
CEN1B
CEN6B
CEN7D
CS
Dt1BL
Dt6BL
Dt7DS
Dt7DL
-200
-100
0
100
200
-4
-2
0
2
4
F
CRW (n = 771)
CS
Dt
CENH3 Enrichment
R = 0.98
-5.0
Start
End
5.0 kb
G
Pearson correlation coefficient
CS
Dt1DS
Dt1AL
Dt7BL
Dt1DL
Dt6AS
Dt1AS
Dt6DS
Dt7AL
Dt7DS
Dt1BL
Dt7DL
Dt6AL
Dt6DL
Dt6BL
Dt7BS
1.0
0.2

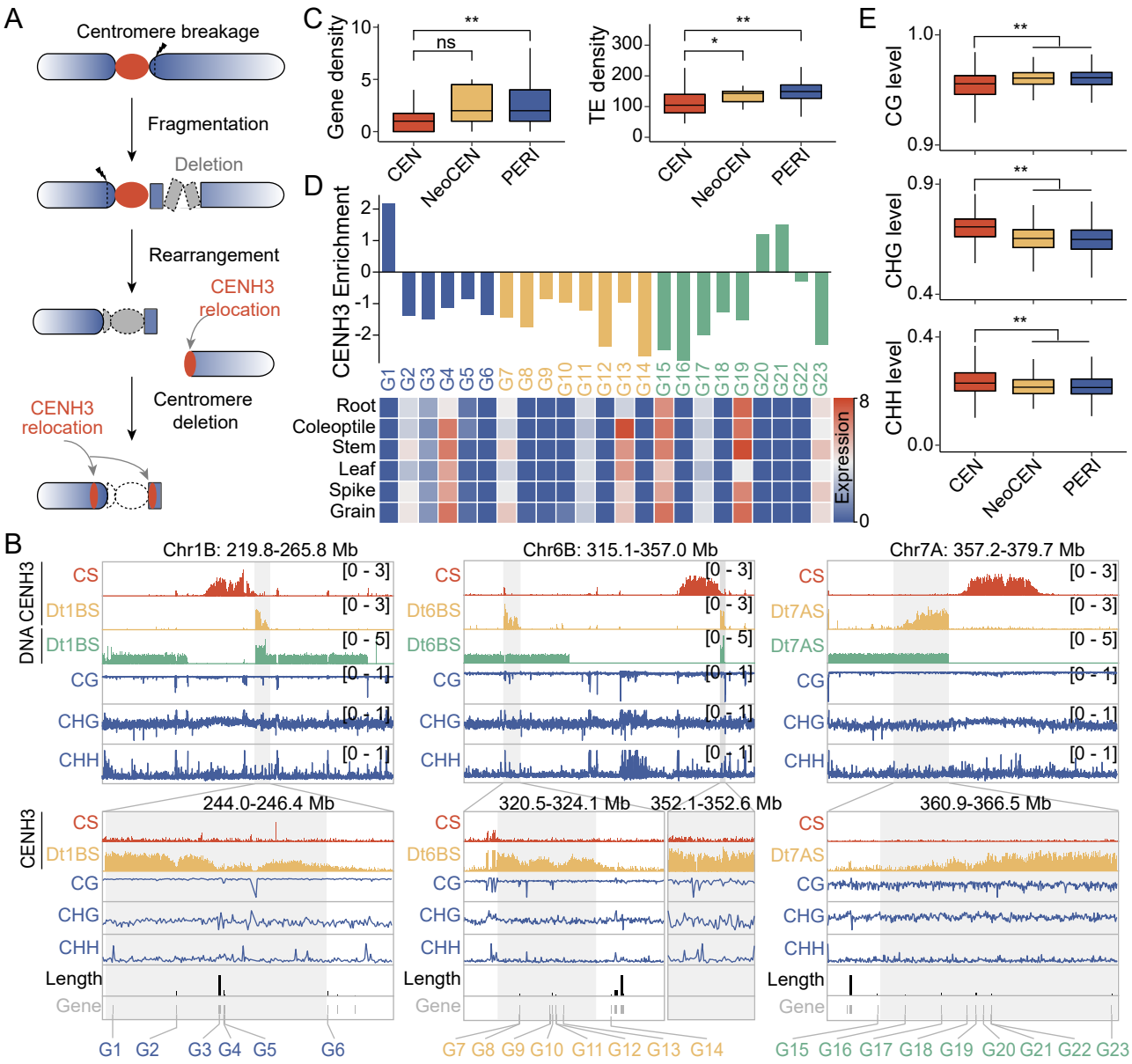
A
Centromere breakage
Fragmentation
Deletion
Rearrangement
CENH3 relocation
Centromere deletion
CENH3 relocation
C
Gene density
TE density
ns
**
*
CEN
NeoCEN
PERI
D
CENH3 Enrichment
G1 G2 G3 G4 G5 G6 G7 G8 G9 G10 G11 G12 G13 G14 G15 G16 G17 G18 G19 G20 G21 G22 G23
Root
Coleoptile
Stem
Leaf
Spike
Grain
Expression
E
CG level
CHG level
CHH level
B
Chr1B: 219.8-265.8 Mb
Chr6B: 315.1-357.0 Mb
Chr7A: 357.2-379.7 Mb
DNA CENH3
CS
Dt1BS
Dt6BS
Dt7AS
CG
CHG
CHH
CENH3
244.0-246.4 Mb
320.5-324.1 Mb
352.1-352.6 Mb
360.9-366.5 Mb
Length
Gene
G1 G2 G3 G4 G5 G6
G7 G8 G9 G10 G11 G12 G13 G14
G15 G16 G17 G18 G19 G20 G21 G22 G23

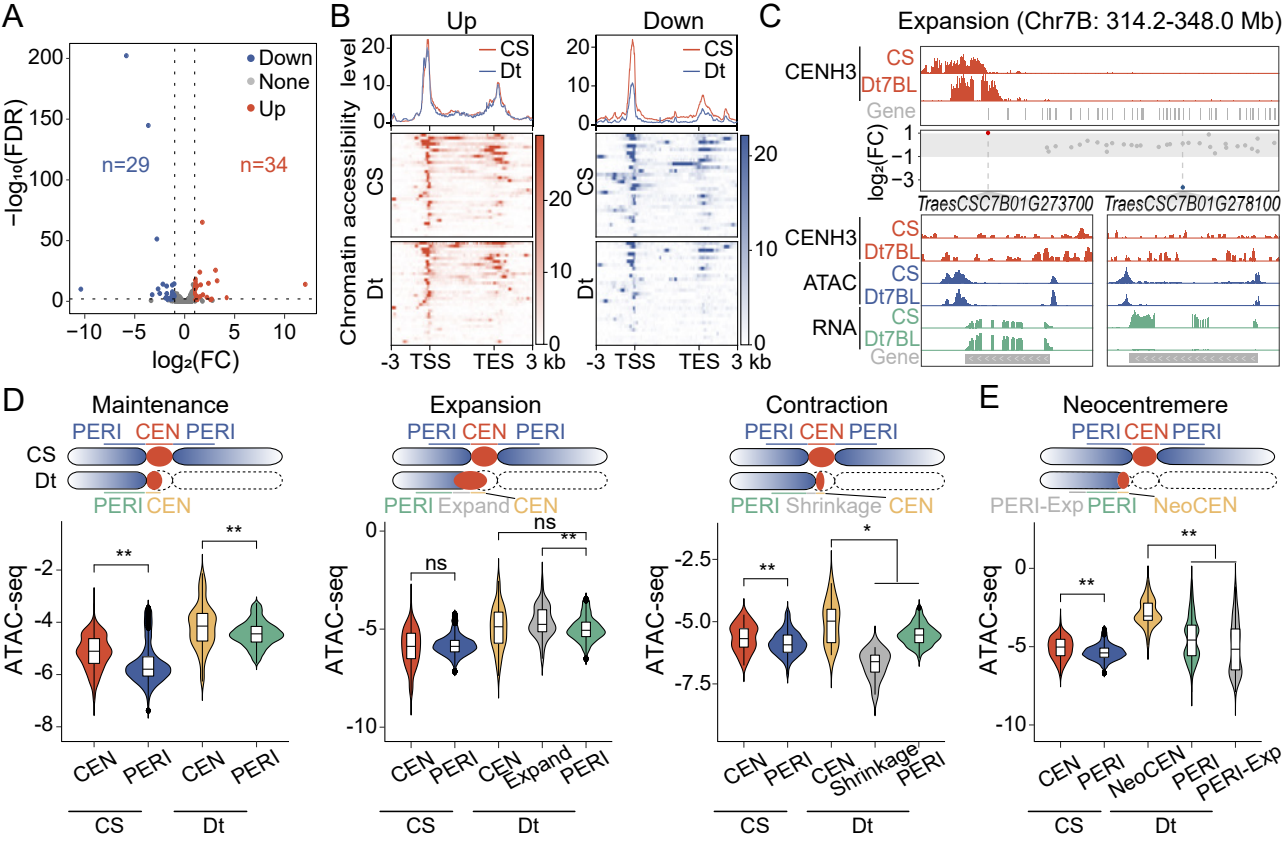
A
Down
None
Up
n=29
n=34
−log10(FDR)
log2(FC)
B
Up
Down
CS
Dt
level
Chromatin accessibility
-3 TSS TES 3 kb
C
Expansion (Chr7B: 314.2-348.0 Mb)
CENH3
Gene
log2(FC)
TraesCSC7B01G273700
TraesCSC7B01G278100
ATAC
RNA
D
Maintenance
Expansion
Contraction
PERI CEN PERI
PERI Expand CEN
PERI Shrinkage CEN
ATAC-seq
ns
CEN
PERI
Expand
Shrinkage/
E
Neocentremere
PERI-Exp PERI NeoCEN
NeoCEN
PERI-Exp

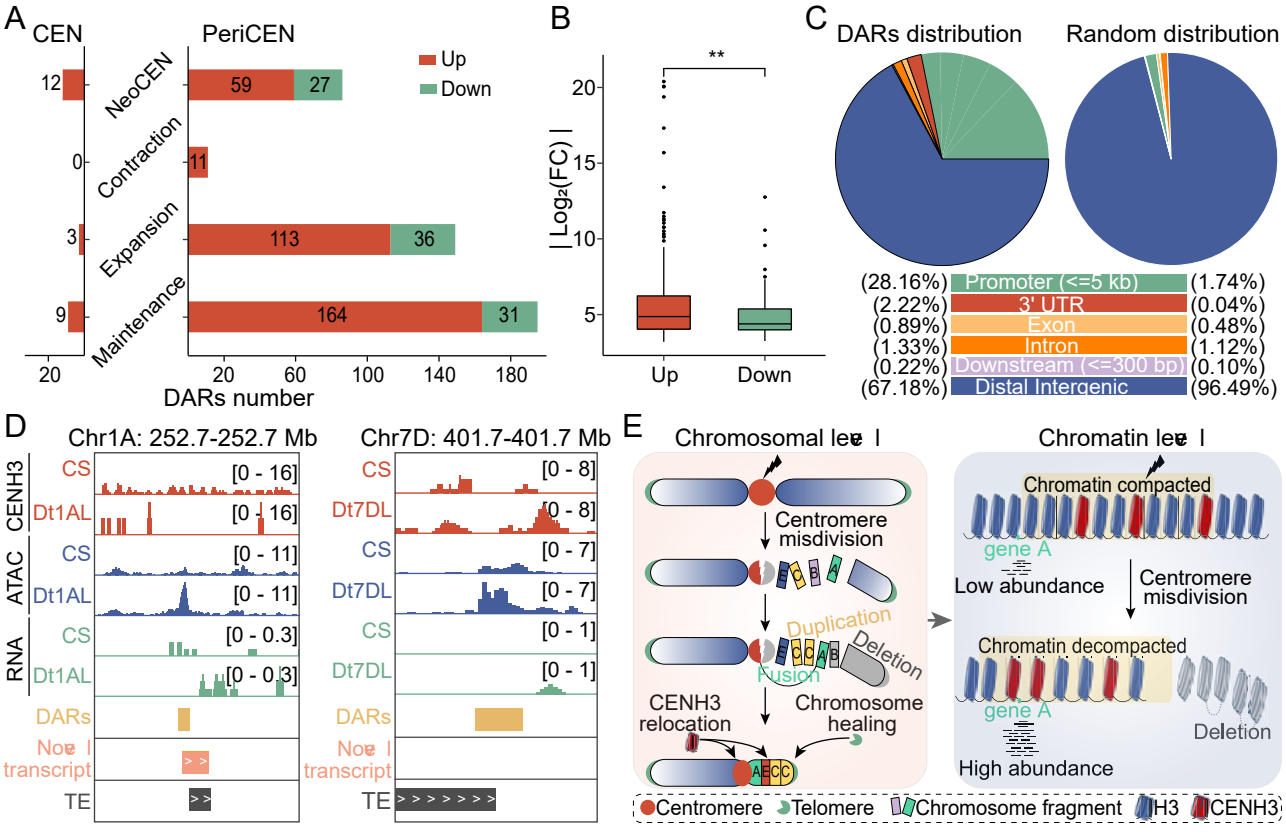
A
CEN
PeriCEN
Up
Down
12
0
3
9
NeoCEN
Contraction
Expansion
Maintenance
59
27
11
113
36
164
31
20
20
60
100
140
180
DARs number
B
**
|Log2(FC)|
20
15
10
5
Up
Down
C
DARs distribution
Random distribution
(28.16%)
Promoter (<=5 kb)
(1.74%)
(2.22%)
3' UTR
(0.04%)
(0.89%)
Exon
(0.48%)
(1.33%)
Intron
(1.12%)
(0.22%)
Downstream (<=300 bp)
(0.10%)
(67.18%)
Distal Intergenic
(96.49%)
D
Chr1A: 252.7-252.7 Mb
Chr7D: 401.7-401.7 Mb
CENH3
ATAC
RNA
CS
Dt1AL
Dt7DL
[0 - 16]
[0 - 11]
[0 - 0.3]
[0 - 8]
[0 - 7]
[0 - 1]
DARs
Novel transcript
TE
E
Chromosomal level
Centromere misdivision
Duplication
Deletion
Fusion
CENH3 relocation
Chromosome healing
Chromatin level
Chromatin compacted
gene A
Low abundance
Centromere misdivision
Chromatin decompacted
High abundance
Centromere
Telomere
Chromosome fragment
H3
CENH3